Electrically Pumped Metallo-Dielectric Pedestal Nanolasers

Qing Gu*, Brett Wingad*, Felipe Vallini**, Boris Slutsky*, Michael Katz*, Maziar P. Nezhad*, Newton C. Frateschi** and Yeshaiahu Fainman*

* Department of Electrical and Computer Engineering, University of California at San Diego, La Jolla, CA 92093, USA

** Department of Applied Physics, "Gleb Wataghin" Physics Institute, University of Campinas - UNICAMP, 13083-859 Campinas, SP, Brazil

Abstract

Electrically pumped metallo-dielectric nanolasers are demonstrated. Employing a two-step InP chemical etching, we obtain straight pedestal sidewalls and preferentially reduce the diameter of the n-doped InP cladding more than the p-doped one for optimized performance.

I. Introduction

The pursuit of electrically pumped semiconductor nanolasers has been of great interest not only for fundamental physics but also as an essential building block for highly integrated photonic circuits [1]. Recently, we reported optically pumped subwavelength metallo-dielectric lasers operating at room temperature [2] and the electrically pumped version operating up to 140K [3], both using a cavity design with a high refractive index contrast between the gain and cladding layers as well as a thin dielectric shield positioned between the gain and the metallic layer.

In this report, we present a combined consideration of optical, electrical and thermal performances which, when optimized, will realize electrically pumped metallo-dielectric nanolasers operating at room temperature.

II. Cavity Design and Modeling

The platform for our devices is an InGaAs/InP double heterostructure grown on InP. The schematic of the device is depicted in Fig. 1(a). The intrinsic 300nm thick (h_{core}) bulk InGaAs layer serves as the active medium. The upper and lower InP layers are doped cladding layers acting as electrical channels through which the injected carriers flow into the active region. Highly doped InGaAsP layers above and below the cladding layers form contact layers. Although the schematic shows a material stack in which the upper layers are n-doped and lower layers are p-doped, similar to the structure reported in [3], we also design devices using a material stack with an inverted doping profile. The SiO_2 shield layer between the gain medium and the metal coating surrounding the cavity serves to minimize the overlap between the optical mode and the metal [2], while the pedestal geometry further enhances the optical confinement in the vertical direction without increasing the pillar height [3]. In our previous design, we had assumed straight pedestal sidewalls and the same reduction of radius (Δr) of the upper and lower cladding layers. However, cone shaped cladding layers resulted due to anisotropic properties of the etchant. Furthermore, due to material-selectivity of the etchant, the cladding layers of different doping types inevitably have different radii.

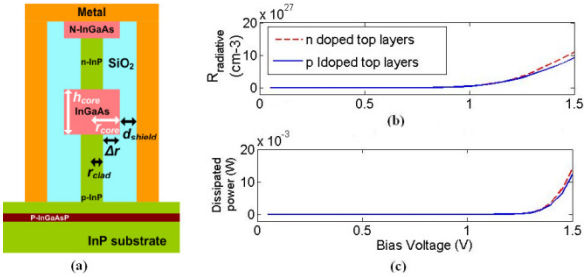

Fig. 1: (a) Schematic of the device, (b) Simulated radiative recombination rate in the active medium and (c) power dissipation of a device with r_{core}=500nm, Δr_{upper}=Δr_{lower}=0nm, d_{shield}=200nm

COMSOL multiphysics software is used for Finite Element Method (FEM) modeling of the optical mode of the structures. For comparison, we numerically model the pedestal structure without reduction of the cladding radii, with the same reduced cladding radii, or with the radius of only one cladding layer reduced. The resulting transparent cavity Q and threshold gain g_{th} are shown in Table 1. We observe that the reduction of the upper cladding radius worsens the optical performance of the device while the reduction of the lower cladding radius improves it. Simultaneous reduction of both radii has a combined effect. SILVACO design software is used for electrical simulations. Using a geometry with r_{core} of 500nm, d_{shield} of 200nm, both Δr_{upper} and Δr_{lower} of 0nm, Fig. 1(b) and (c) show respectively the radiative recombination rate in the active medium and the dissipated power of the device, where the top layers are either n doped (red dotted curve) or p doped (blue curve).

Table 1: Simulated cavity Q and threshold gain for different cladding configuration of the nanolaser with r_{core}=210nm, pillar d_{shield}=70nm

Δr_{upper}	0	50	50	0
Δr_{lower}	0	50	0	50
Cavity Q	242	815	142	909
g_{th} (cm^{-1})	1106	233	1900	270

Even though cavity Q and threshold gain improve as the cladding radii decreases, carrier transport becomes harder, corresponding to increased device resistance and heat generation, detrimental for continuous wave (CW) operation. Therefore, an optimized set of cladding radii exist for each gain core radius, providing optimal optical and electrical performance of the device.

978-1-4673-6476-8/13/$31.00 ©2013 IEEE

III. Fabrication and Measurement

The initial circular masks for the pillars are created by e-beam lithography with hydrogen silsesquioxane (HSQ) negative resist. Subsequent reactive ion etch (RIE) is used to form circular pillar structures of 1.4um height, as shown in Fig. 2(a). We employ a two-step InP wet etching process to obtain straight pedestal sidewalls of the InP cladding layers [4]. In the first step of the selective etching, the $HCl:H_3PO_4$ (1:4) etchant combination is used, whose anisotropy in the <011> orientation leads to a cone shaped cladding layer, as depicted in Fig. 2(b). In the second step, the HCl:CH3COOH (1:4) combination is used, which also has anisotropy in the <011> orientation but leads to a cone shaped cladding layer in the opposite direction if used alone, as shown in Fig. 2(c). Therefore, using the two chemistries sequentially with the proper ratio of etching times, we obtain straight inner pedestal pillar sidewalls as shown in the inset of Fig. 2(a). We observe that the etching rate is different for different doping types. Therefore, for structures with p type doping on top, we obtain a narrower bottom cladding radius than the n top one. Fig. 2(d) and (e) show the pedestal pillars after the two-step etching process for material platforms with n type and p type doping on top, respectively.

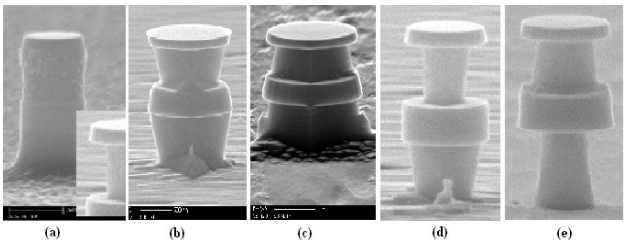

Fig. 2: SEM images of pedestal pillar lasers (a) before (inset: after) the 2-step wet etching, (b) after $HCl:H_3PO_4$ etch, (c) after HCl:CH3COOH etch, (d) Pedestal nanolasers with n doped top layers and (e) with p doped top layers, after the 2-step wet etching.

After selective etching of the cladding layers, similar to the steps taken in Lee et. al [3], the SiO_2 shield layer is deposited around the pillar and substrate, and silver is deposited as the cavity metal around the shielded pillar. Metal contacts (Ti/Pd/Au) are formed through multiple photolithography, metal deposition, lift-off and annealing processes. Finally, the sample is mounted on a commercial chip package (TO 8) and wire-bonded.

To measure, the laser device is forward biased by a DC voltage source operating up to 5V, and CW emission from the device is collected through a 20x objective lens into a monochrometer for spectral measurements. Fig. 3 shows characterization results at 77K of a device with n-doped top layers, whose core radius is 750nm, SiO_2 shield thickness is 130nm, with Δr_{upper} of 185nm and Δr_{lower} of 90nm. Fig. 3(a) depicts the spectral evolution of emission: from a broad-band electroluminescence at low injection current to narrow lasing peaks at high injection currents, with a lasing linewidth of 0.4nm, as shown in the inset of Fig. 3(b). The light output-injection current (L-I) curve is depicted in Fig. 3(b). Note that the shield thickness is not optimized for the device.

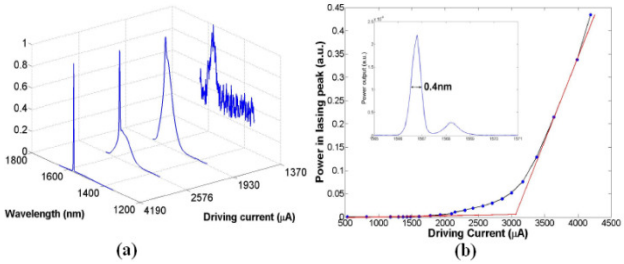

Fig. 3: Lasing characteristics at 77K of a device with r_{core}=750nm, Δr_{upper}=185nm, Δr_{lower}=90nm and d_{shield}=130nm. (a) Spectrum evolution and (b) L-I curve, inset: lasing linewidth.

IV. Conclusions

Electrically pumped metallo-dielectric pedestal nanolasers are designed and demonstrated experimentally in CW operation. Through a two-step InP selective etching process, we improve the device's optical performance without increasing the device dimension. Utilizing the anisotropy of different etchants, we obtain straight pedestal sidewalls with good morphology; while utilizing the material-selectivity of the etchants, we preferentially reduce the diameter of one cladding layer more than the other for optimized device performance. Furthermore, better thermal management can be achieved in the future by replacing the SiO_2 shield with Al_2O_3. The optimization among optical, electrical and thermal performances presents a promising approach towards room temperature operation.

Acknowledgment

This work was supported by the Defense Advanced Research Projects Agency (DARPA), the National Science Foundation (NSF), NSF through Center for Integrated Access Networks (CIAN) NSF ERC under grant #EEC-0812072, the Cymer Corporation, the U.S. Army Research Office. This work is also partly supported by the Brazilian financial agencies: FAPESP, CNPQ, CAPES and is done within the National Institute for Science and Technology (FOTONICOM).

References

[1] K. Ding and C. Ning, "Metallic subwavelength-cavity semiconductor nanolasers," *Light: Science & Applications,* vol. 1, pp. e20, 2012.

[2] M. P. Nezhad, A. Simic, O. Bondarenko, B. Slutsky, A. Mizrahi, L. Feng, V. Lomakin and Y. Fainman, "Room-temperature subwavelength metallo-dielectric lasers," *Nature Photonics,* vol. 4, pp. 395-399, 2010.

[3] J. H. Lee, M. Khajavikhan, A. Simic, Q. Gu, O. Bondarenko, B. Slutsky, M. P. Nezhad and Y. Fainman, "Electrically pumped sub-wavelength metallo-dielectric pedestal pillar lasers," *Optics Express,* vol. 19, pp. 21524-21531, 2011.

[4] E. Inamura, Y. Miyamoto, S. Tamura, T. Takasugi and K. Furuya, "Wet chemical etching for ultrafine periodic structure: rectangular InP corrugations of 70 nm pitch and 100 nm depth," *Japanese Journal of Applied Physics,* vol. 28, pp. 2193-2196, 1989.